nature physics

ARTICLES

https://doi.org/10.1038/s41567-019-0630-5

Half-integer level shift of vortex bound states in an iron-based superconductor

Lingyuan Kong[1,2,7], Shiyu Zhu[1,2,7], Michał Papaj[3,7], Hui Chen[1,7], Lu Cao[1,2], Hiroki Isobe[3], Yuqing Xing[1,2], Wenyao Liu[1,2], Dongfei Wang[1,2], Peng Fan[1,2], Yujie Sun[1,4,5], Shixuan Du[1,4], John Schneeloch[6], Ruidan Zhong[6], Genda Gu[6], Liang Fu[3]*, Hong-Jun Gao[1,2,4]* and Hong Ding[1,4,5]*

Vortices in topological superconductors may host Majorana zero modes (MZMs), which have been proposed as the building blocks of fault-tolerant topological quantum computers. Recently, a new single-material platform with the potential for realizing MZMs has been discovered in iron-based superconductors, without involving hybrid semiconductor–superconductor structures. Here, we report a detailed scanning tunnelling spectroscopy study of a $FeTe_{0.55}Se_{0.45}$ single crystal and show that this material hosts two distinct classes of vortex. These differ by a half-integer level shift in the energy spectra of the vortex bound states. This level shift is directly tied to the presence or absence of a zero-bias conductance peak and also alters the ratios of higher energy levels from integer to half-odd-integer. Our model calculations fully reproduce the spectra of these two types of vortex bound state, suggesting the presence of regions with and without topological surface states, which coexist within the same crystal. Our findings provide strong evidence for the presence of MZMs in $FeTe_{0.55}Se_{0.45}$ and establish it as an excellent platform for further studies.

Majorana zero modes (MZMs) are proposed as the building blocks of fault-tolerant topological quantum computation[1] due to their non-Abelian statistics. Several systems are predicted to host MZMs, such as intrinsic *p*-wave superconductors[2,3] and multiple heterostructures combining strong spin–orbital coupling (SOC) and superconductivity[4–12]. Recently, a new single-material platform composed of iron-based superconductors (FeSCs) has been discovered[13–15] in which topological non-trivial bands and high-temperature (high-T_c) superconductivity coexist naturally[16] without the need for the proximity effect common to other arrangements. This has led to the observation of a pronounced zero-bias conductance peak (ZBCP) in vortices of $FeTe_{0.55}Se_{0.45}$ (ref. [17]) and a related compound[18].

Although a ZBCP that does not split across the vortex core is regarded as a strong indication of MZMs and the topological nature of the superconducting vortex[4,17–19], the observation of ZBCPs alone is not enough to prove it. Although several pieces of evidence, including spatial profile, tunnelling barrier dependence, magnetic field dependence and temperature evolution, are fully consistent with a MZM in $FeTe_{0.55}Se_{0.45}$ (ref. [17]), a more convincing verification is required in the form of a demonstration of the non-trivial topology of the superconducting vortex and underlying band structure. Single-crystal $FeTe_{0.55}Se_{0.45}$ is a unique platform for demonstrating the fundamental distinction between trivial and topological vortices. Its large ratio[17,20] Δ/E_F (Δ being the superconducting gap, E_F being the Fermi energy) enables realization of the quantum limit[21], where the low-lying quasiparticle bound states, the so-called Caroli–de Gennes–Matricon bound states (CBSs)[22], become discrete levels observable separately within the hard superconducting gap. These bound states are the eigenstates of the vortex planar angular momentum[21–23], with eigenvalues determined by the topological phase of the vortex line[4,24]. Even though topology dictates the existence of two types of discrete bound state spectrum, in ordinary circumstances a given material belongs to just one of the classes. This restricts a single sample to one type of spectrum and thus forbids a direct comparison. However, the intrinsic inhomogeneity of $FeTe_{0.55}Se_{0.45}$ (refs. [25–28]), while reducing the number of vortices that host MZMs[17], provides a rare opportunity to observe topological and ordinary vortices simultaneously in the same material or even the same region, thus making such a comparison feasible.

Here, we report a systematic scanning tunnelling microscopy/spectroscopy (STM/S) study of vortices in $FeTe_{0.55}Se_{0.45}$. We observe two topologically distinct classes of vortex, which differ not only in the presence or absence of ZBCPs, but also in the quantization sequence of the remaining higher-energy subgap states. Our analysis compares and contrasts multiple vortices that belong to these two classes and reveals that the ratios of bound state energy follow either integer or half-odd-integer numbers, provided that the chemical potential is not too small compared to the superconducting gap. This fundamental difference, arising due to an additional angular momentum contribution, is accounted for by our model calculation, which reproduces the discrete bound state spectra and allows us to identify the integer-spaced levels as emerging from topological surface states. In contrast, in an ordinary vortex without MZM, the discrete CBS energies have half-odd-integer spacing, reflecting the trivial topology of the underlying band structure. This half-integer level shift of the vortex bound states between two distinct classes of vortex provides strong evidence for the existence of a pure Majorana

[1]Beijing National Laboratory for Condensed Matter Physics and Institute of Physics, Chinese Academy of Sciences, Beijing, China. [2]School of Physical Sciences, University of Chinese Academy of Sciences, Beijing, China. [3]Department of Physics, Massachusetts Institute of Technology, Cambridge, MA, USA. [4]CAS Center for Excellence in Topological Quantum Computation, University of Chinese Academy of Sciences, Beijing, China. [5]Songshan Lake Materials Laboratory, Dongguan, Guangdong, China. [6]Condensed Matter Physics and Materials Science Department, Brookhaven National Laboratory, Upton, NY, USA. [7]These authors contributed equally: Lingyuan Kong, Shiyu Zhu, Michał Papaj, Hui Chen. *e-mail: liangfu@mit.edu; hjgao@iphy.ac.cn; dingh@iphy.ac.cn

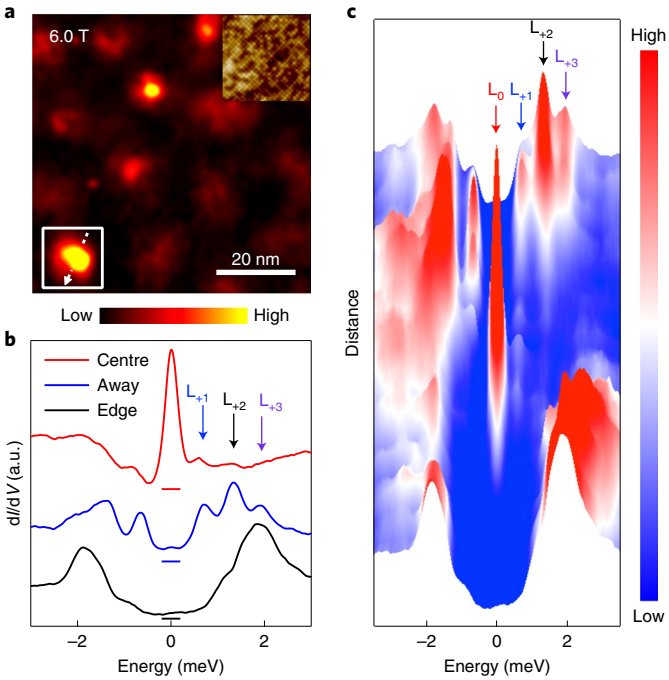

Fig. 1 | CBSs in a vortex with MZM. a, A normalized zero-bias conductance map measured at a magnetic field of 6.0 T (area of 70 × 70 nm^2). The average inter-vortex length is ~19.3 nm, which is consistent with the expectation $L = \sqrt{2\Phi_0/\sqrt{3}B}$. Inset: STM topography of $FeTe_{0.55}Se_{0.45}$ (scanning area of 10 × 10 nm^2; sample bias $V_s = -5$ mV, tunnelling current $I_t = 0.2$ nA). **b**, Typical tunnelling conductance spectra measured around the vortex marked by the white box in **a**. The curves are offset for clarity. The red curve is measured at the vortex centre. The blue curve is measured slightly off centre and the black curve is measured at the vortex edge. The short coloured bar below each curve marks its zero conductance. **c**, Three-dimensional (3D) display of the line-cut intensity plot along the white dashed line in **a**. Four subgap states are identified by arrows in different colours. Besides the MZM, all the CBSs almost remain at the same energy along the line cut through the vortex.

zero mode in the FeSC material. Our results also provide a detailed understanding of vortex bound states in $FeTe_{0.55}Se_{0.45}$ and in this way facilitate future applications of MZMs in this material platform.

Integer quantized CBSs in a topological vortex core

To investigate the vortex bound state spectra experimentally, we performed low-temperature ($T_{exp} = 0.55$ K), high-resolution (0.28 meV) STM/S measurements on as-grown superconducting $FeTe_{0.55}Se_{0.45}$ single crystals ($T_c = 14.5$ K). An atomically resolved lattice structure is observed on the in situ cleaved surface (inset, Fig. 1a). When the magnetic field exceeds H_{c1}, superconducting vortices appear as the material enters the mixed state typical of the type II superconductor[29]. With a 6.0 T magnetic field applied perpendicular to the sample surface, we find multiple vortices in the zero-bias conductance map shown in Fig. 1a. In the centre of the vortex core, there are sharp ZBCPs with a full-width at half-maximum that is almost resolution- and temperature-limited (Supplementary Fig. 1a,b). In our previous work[17], we provided evidence that this ZBCP is a Majorana zero mode induced by the surface Dirac fermions observed in high-resolution angle-resolved photoemission spectroscopy (ARPES) measurements[16]. In this study, we highlight additional high-energy subgap features in the spectrum that are crucial in distinguishing between the topological and trivial nature of superconducting vortices and the underlying band structure. To obtain a better understanding of the origin of these subgap features, it is beneficial to focus on the vortices where there are several visible peaks inside the gap. This situation corresponds to vortices present in a region where Δ/E_F is smaller, but not too small, to guarantee the presence of several subgap levels with discrete spectra observable under the quantum limit[21]. For such a vortex, the spectrum measured slightly off centre (blue curve, Fig. 1b) shows three high-energy bound states that coexist with the MZM. We find that, similar to the MZM, the non-zero energy bound states also do not shift when we change the spatial position of the STM tip (Fig. 1c). The discrete features in the spectrum (for which the energy does not shift along the real space cut) are characteristic of CBSs in the quantum limit[21], as observed previously[30]. The strong electron correlation in this material[31] leads to a large Δ/E_F, thus enabling our experiments well below the required temperature ($T_{exp} < T_{QL} = T_c\Delta/E_F$).

We next examine the level spacing of these discrete CBSs coexisting with a MZM (Fig. 2). We extract the energy positions of each level (Fig. 2c) using a Gaussian fit (Fig. 2b). We identify six discrete levels marked by L_0, $L_{\pm1}$, $L_{\pm2}$, L_{+3}, with energy values of 0, 0.65, 1.37 and 1.93 meV, respectively (Supplementary Fig. 1d). It is clear that the CBSs are almost equally spaced in energy. Using the energy of the first level as the energy unit, we present a histogram for each of the levels in Fig. 2d and show that the ratio of the energy levels ($E_L/\Delta E$) closely follows the form 0:1:2:3. The integer quantized CBSs can also be visualized in the overlap plot in Fig. 2e, which shows several peaks that do not shift in space and that coexist with the sharp MZM. We summarize the energy level ratios of seven different vortices in which a MZM is observed in Fig. 2f. Although the absolute level energies vary slightly from vortex to vortex (Supplementary Fig. 2), the normalized energy in units of the first energy level converges to a straight line of integer quantization for all of the vortices present in such regions. This suggests that, although the CBS energy values in those vortices are influenced by the local environment, the integer quantized property is robust, as long as the topological nature of the underlying band structure remains intact (see additional set of data measured under 40 mK and 2.0 T in Supplementary Fig. 9a,b).

We support this conclusion with an energy spectrum calculation using the Fu–Kane model[4,17] (for details see Supplementary Section IV). We present a comparison of the observed peak positions and calculated energy eigenvalues of the vortex bound states (Supplementary Fig. 5f). The excellent agreement provides strong evidence for the topological nature of vortices in $FeTe_{0.55}Se_{0.45}$, demonstrating that the integer quantized CBS levels are the direct consequence of the topological surface states. In our previous work[17], we focused on vortices with larger level spacing between the MZM and first vortex bound state at non-zero energy. Our calculation also reproduces its spectrum precisely when we decrease the value of the chemical potential (Supplementary Fig. 5e). This shows that, in the case of the chemical potential being very close to the Dirac points, a large level spacing will push the first non-zero energy bound state very close to the energy of the superconducting gap, and thus the integer quantization of CBS levels is broken down by quantum confinement effects[32]. We also note that the energy of the Dirac point is a 'sweet spot' for quantum computation. If the chemical potential is located exactly at such a point, a MZM is the only allowed subgap state in a topological vortex core[32–34], and all the other non-zero bound states are pushed to the superconducting gap edge (Supplementary Section III and Supplementary Fig. 5). The larger level spacing between the MZM and the first CBS in this material, especially when the material approaches the zero doping limit[32–34] (Supplementary Fig. 6), protects the MZM from external perturbations[35], which is favourable for the demonstration of non-Abelian statistics of MZMs in a braiding operation[1,36].

Half-odd-integer quantized CBSs in an ordinary vortex core

However, in our samples there exists another class of vortices that do not contain MZMs. To examine their origin, we repeat the

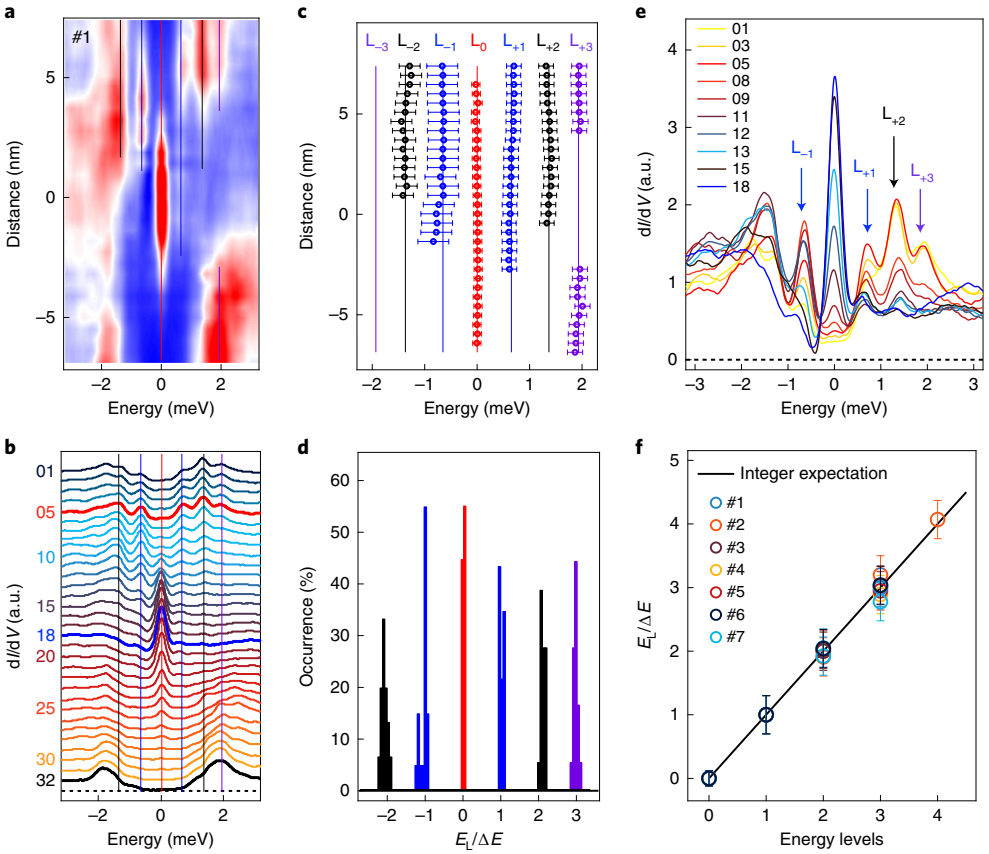

Fig. 2 | Integer quantized CBSs in a topological vortex. a, A line-cut intensity plot of topological vortex #1, showing discrete quantized CBSs (marked by coloured solid lines). **b**, A waterfall-like plot of **a** with 32 spectra. Spectra numbers are marked on the left. Curves in red, blue and black are shown in Fig. 1b in the same colours. **c**, The energy values of the observed CBSs at different spatial positions. The energies of the CBSs, labelled L_0, $L_{\pm1}$, $L_{\pm2}$, L_{+3}, are extracted from **b** with a Gaussian fit. Error bars are calculated as the s.d. of each energy level. The s.d. of the MZM is 0.08 meV, smaller than the lock-in modulation energy used in the experiments, $eV_{mod} = 0.1$ meV. The energy values of the solid lines are calculated as the average energy of each level. **d**, Histogram of the energy values of all the observed subgap states. The sampling width is 40 μeV. The energy of the horizontal axis is normalized by the first level spacing, that is, the ratio $E_L/\Delta E$. **e**, An overlapping plot of 10 dI/dV spectra selected from **b**. **f**, Summary of $E_L/\Delta E$ versus level number data for topological vortices #1 to #7. This demonstrates that the CBS energies are proportional to integers. The solid line is calculated using $E_L/\Delta E = E_L/(\Delta^2/E_F) = n$, where n is the number of energy levels. The error bars for the L_0 levels are calculated by dividing the s.d. of L_0 (shown in **c**) by ΔE, while the bars for the other levels are calculated by dividing the averaged s.d. by ΔE.

analysis from the previous section for the CBSs in these ordinary vortices. Similar to the case of a topological vortex, CBSs in the ordinary vortex are discrete in energy (Fig. 3). The first CBS level (L_{+1}) is located at 0.26 meV. The energies of higher levels (L_{+2}, L_{+3}, L_{+4}, L_{+5}) are found to be 0.83, 1.34, 1.84 and 2.34 meV, respectively. These CBSs show a strong particle–hole asymmetry, being strong in positive energy and very weak in negative energy (Fig. 3b). This particle–hole asymmetry is a common phenomenon for the superconducting vortex core of FeSC materials[37,38], although the degree of asymmetry varies for different vortices (see Supplementary Fig. 4 for more examples measured at 550 mK and Supplementary Fig. 9c,d for an additional set of data measured under 40 mK and 2.0 T that has more clearly visible particle–hole symmetric peaks at negative energies).

Although we cannot locate the L_{-1} level of the CBSs in Fig. 3, the absence of the ZBCP indicates that no bound state in the vortex has an angular momentum eigenvalue equal to zero. By using the first level spacing as a unit, we summarize the ratios ($E_L/\Delta E$) of the three vortices in Fig. 3d. Despite a strong variation in particle–hole asymmetry among these vortices, the ratios converge into a straight line of half-odd-integer quantization with the form 0.5:1.5:2.5:3.5:4.5. The appearance of CBSs with energy values proportional to half-odd integers in a vortex without a ZBCP is consistent with the expected behaviour of an ordinary vortex core in which only the pairing in conventional bands contributes to the quasiparticle excitations under a magnetic field[21–23,39]. The angular momentum eigenvalues of the bound states in an ordinary vortex are half of an odd integer. Accordingly, the energies of CBSs inherit the half-odd-integer quantization with an equal level spacing close to the centre of the gap. In this case we also provide a numerical calculation of the energy spectrum based on solving the Bogoliubov–de Gennes equation with parabolic conventional bands that reproduces the experimental energy values (for details see Supplementary Fig. 3).

Characteristic spatial pattern of the quantized CBSs

Friedel-like oscillation of the local density of states has been predicted in half-odd-integer quantized CBSs of an ordinary vortex core, with the spatial periodicity being approximately on the scale of the Fermi wavelength of order $1/k_F$ (refs. [21,40]). The typical k_F of conventional bands is larger than 0.1 A^{-1} (ref. [41]), leading to the spatial oscillations of CBSs within 1 nm in an ordinary vortex core, which is difficult to observe by STM[29,30,37–39] (see Supplementary Fig. 11 for an example). However, in $FeTe_{0.55}Se_{0.45}$, a minimal value of k_F on the order of 0.01 A^{-1} was observed for its Dirac surface state[16].

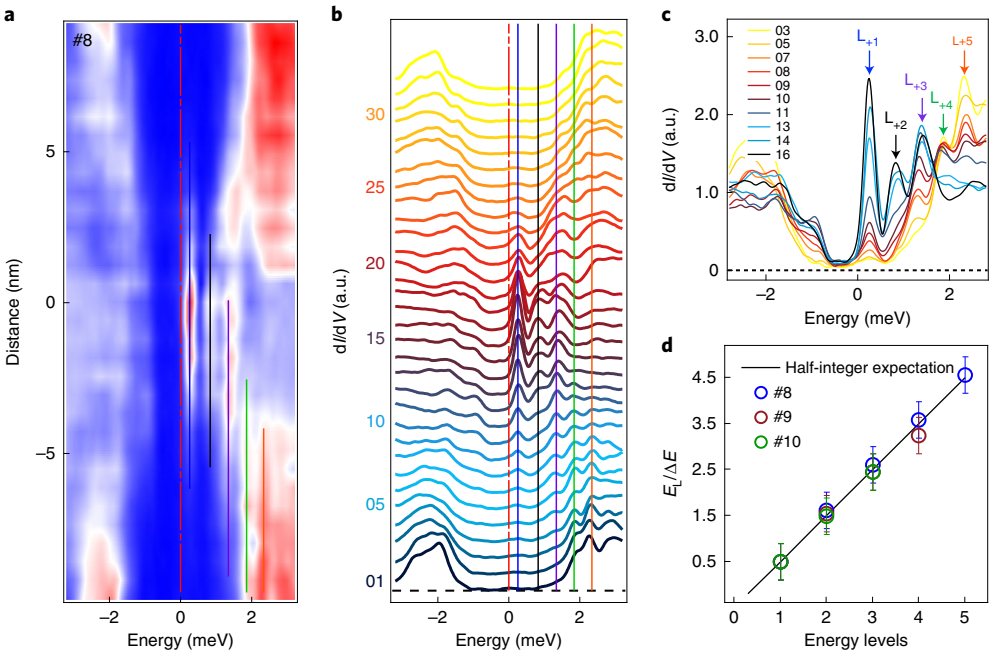

Fig. 3 | Half-odd-integer quantized CBSs in an ordinary vortex. a, A line-cut intensity plot of ordinary vortex #8, where the CBSs are marked by solid coloured lines. **b**, A waterfall-like plot of **a** with 32 spectra. Spectra numbers are marked on the left. **c**, An overlapping plot of 10 d*I*/d*V* spectra from **b** with the energy levels of the CBSs labelled L_{+1}, L_{+2}, L_{+3}, L_{+4}, L_{+5}. **d**, Summary of $E_L/\Delta E$ versus level number data for ordinary vortices #8 to #10. ΔE is determined as double the energy of the lowest level. This demonstrates that the CBS energies are proportional to half-odd integers. The solid line is calculated using $E_L/\Delta E = E_L/(\Delta^2/E_F) = (2n-1)/2$, where n is the number of energy levels. Error bars are calculated by dividing the averaged s.d. by ΔE.

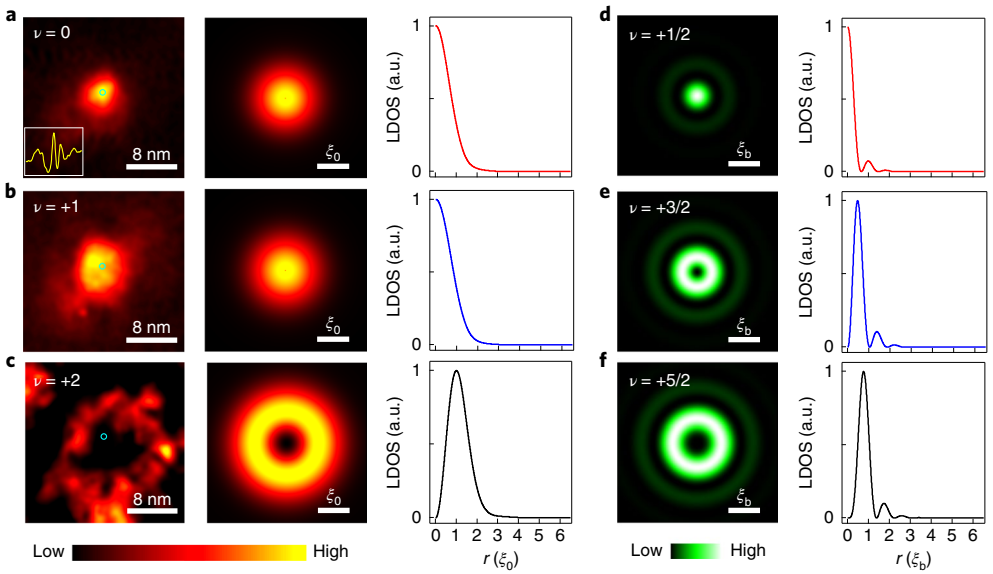

Fig. 4 | Spatial pattern of integer quantized CBSs. a–c, Comparison plots of STM measurements and numerical calculations for a topological vortex, L_0 (MZM), L_{+1} and L_{+2}, respectively. The inset in **a** is a typical STS spectrum measured at a vortex centre, with integer quantized CBS levels located at 0.6, 1.3 and 1.8 meV for L_{+1}, L_{+2} and L_{+3}, respectively. Left column: constant bias conductance maps of each CBS level (area of $25\times25\,nm^2$), where the cyan symbols marked on the three images are the locations of the vortex centres extracted from **a**. The MZMs (L_0) and the first CBS level (L_{+1}) have the strongest intensity at the vortex centre; however, the second CBS level shows a ring-like feature around the vortex centre, with an offset. The radius of the ring (R) is ~7 nm, which corresponds to the value of Fermi momentum $k_f \approx 1/R \approx 0.014\,Å^{-1}$, similar to the results of ARPES measurements on the Dirac surface states. Middle column: numerical calculations of the 2D local density of states (LDOS) based on the model we constructed to simulate a topological vortex core (for details see Supplementary Section IV). Right column: the radial wavefunction of each level. **d–f**, Numerical calculations for an ordinary vortex, for L_{+1}, L_{+2} and L_{+3}, respectively. The left and right columns show numerical calculations of the 2D LDOS and radial wavefunction, respectively. In this case, only one level shows an intensity maximum at the vortex centre, which is in stark contrast to the case of the topological vortex. ν, eigenvalue of angular momentum; ξ_0 and ξ_b, characteristic length calculated from the surface state and bulk bands, respectively.

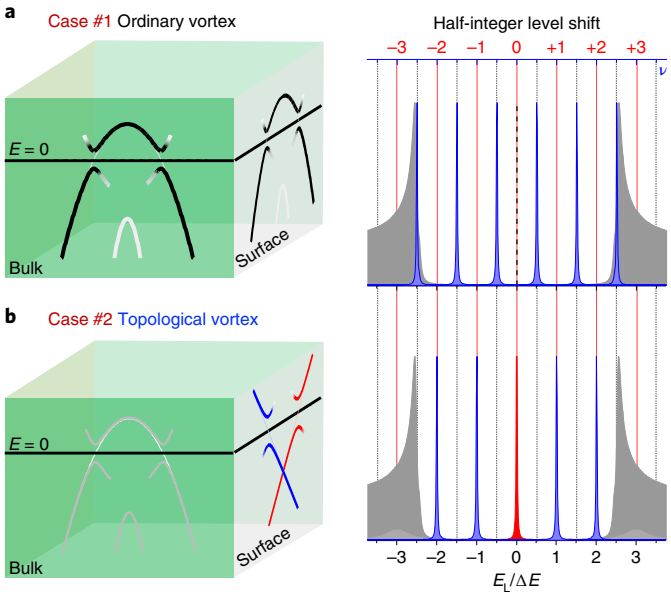

Fig. 5 | Half-integer level shift around a MZM. Left: schematic plots of the underlying surface and bulk band structure for different cases. Right: schematic plots of the subgap CBSs. The blue axis marks the eigenvalues of vortex planar angular momentum. **a**, When the underlying band structure is topologically trivial, the vortices behave ordinarily. The bulk bands with spin degeneracy dominate quasiparticle excitations inside the vortex. Due to the absence of Dirac electrons on the sample surface, quasiparticles can only feel the phase winding of the ordinary superconducting vortex, which leads to half-odd-integer angular momenta and related half-odd-integer quantized CBSs. **b**, When the underlying band structure is dominated by the topological surface state, vortex quasiparticle excitations gain an additional angular momentum from the Dirac electrons. This induces a half-integer level shift of those CBSs as compared with **a**, and the zero-energy bound state becomes a MZM due to the effective spinless *p*-wave-like pairing induced on the Dirac surface states. If the chemical potential in **b** is tuned to the Dirac point, which is the zero doping limit, all the CBSs are pushed towards the gap edge, leaving the MZM isolated at zero energy (for details see Supplementary Fig. 6).

Therefore, the resulting large oscillation periodicity enables easier observation of the spatial pattern of CBSs by STM. As a final piece of evidence for the topological nature of the vortices that contain ZBCPs, we perform a constant-bias conductance mapping of the three lowest levels of the integer quantized CBSs (Fig. 4). Although the ZBCP and the first-level CBS (L_{+1}) display a solid circle spatial pattern around the centre of the vortex core (left, Fig. 4a,b), the second-level CBS (L_{+2}) shows a hollow ring pattern around the vortex centre (left, Fig. 4c). This pattern is unique to Dirac fermions of topological surface states with spin-momentum locking, whereas in ordinary vortices only a single bound state has a wavefunction maximum at the centre of the vortex[21,42] (Fig. 4d–f). The measurement is also fully consistent with our numerical calculation for a topological vortex (middle, Fig. 4a–c) which clearly reveals the difference in the spatial pattern of the wavefunctions of these three levels (right, Fig. 4a–c).

Half-integer level shift between two classes of vortex

We have observed the distinction in the energy spectra of vortex bound states in topological and ordinary vortices. In an ordinary vortex core (Fig. 5a), only the conventional bands contribute to the quasiparticle excitations, and the bound states have eigenvalues of angular momentum that are half-odd integer as a result of the addition of an integer orbital contribution L and half-odd-integer vorticity contribution τ (for vortices with an odd winding number). Accordingly, the energy eigenvalues of CBSs are also approximately half-odd-integer quantized, that is, $E_\nu = \nu\Delta^2/E_F$ ($\nu = \pm 1/2, \pm 3/2, \pm 5/2, \ldots$), where ν is the eigenvalue of angular momentum[21–23]. On the other hand, topological vortices (Fig. 5b) that arise due to superconductivity in Dirac surface states gain an additional half-odd-integer contribution S to the angular momentum due to intrinsic spin carried by Dirac fermions[4,32,42]. This leads to a half-integer shift of the angular momentum, so that it becomes an integer, and the energy values of the bound states are integer quantized by $E_\nu = \nu\Delta^2/E_F$ ($\nu = 0, \pm 1, \pm 2, \pm 3, \ldots$). Majorana zero modes can then be regarded as a special zero-energy CBS for a topological vortex with $\nu = 0$, as long as the zero-energy CBS is an equal-weight mixture of particle/hole components, and the spin degree of freedom is frozen out[24].

Following this discussion, the class to which a vortex belongs can be determined by the nature of the electron states that comprise it, either the Dirac surface states or conventional bulk bands. Considering the intrinsic inhomogeneity[25–28] of $FeTe_{0.55}Se_{0.45}$, which is a telluride/selenide alloy, the character of the electronic states on the surface can vary across the sample. We did find experimentally that the two distinct classes of vortex coexist in a small area within several hundred nanometres (Fig. 1a and Supplementary Fig. 8). We propose that Dirac surface states disappear in some regions of the (001) sample surface, moving deeper into the crystal, but remain intact in other regions (Supplementary Fig. 10a). The coexistence of topological and conventional regions in the same crystal is also supported by our vortex class statistics measurements on the three regions shown in Supplementary Fig. 8 and Supplementary Section V. This analysis demonstrates that the vortices that belong to the same class, either topological or ordinary, usually group together. Theoretically, there are several ways proposed that can eliminate the Dirac surface states on the (001) surface of a strong topological insulator. One mechanism is to drive the material into a trivial insulating/metallic phase by closing the bulk topological gap[43–45]. Another way is to drive the material into a weak topological insulating phase by inducing an even number of topological band inversions at its time-reversal invariant momenta[46–48]. As discussed in the following, both can occur locally in $FeTe_{0.55}Se_{0.45}$.

First, the combined effects of inhomogeneous scattering and the small bulk topological gap can induce trivial insulating or metallic regions in $FeTe_{0.55}Se_{0.45}$. Although it is known that Dirac surface states cannot be destroyed by weak non-magnetic scattering[43] due to the protection by time-reversal symmetry in a Z_2 topological insulator[46], there is a possibility to break down this topological protection by overcoming the bulk topological gap. This gap is very small in $FeTe_{0.55}Se_{0.45}$ (refs. [44,45]), as shown by previous high-resolution ARPES measurements[16] that give an estimate of only ~20 meV, one order of magnitude smaller than the gap in Bi_2Se_3 (ref. [43]). Non-magnetic scattering, such as chemical disorder or impurities beneath the sample surface, can drive the material into a trivial insulating/metallic phase in the vicinity of the scatters, when their potential strength is larger than the topological gap[44,45]. Accordingly, the vortices appearing in the conventional regions are dominated by conventional bands that contain half-odd-integer quantized CBSs. This scenario is consistent with a recent experiment on another compound, $Li_{0.84}Fe_{0.16}OHFeSe$ (ref. [18]), where MZMs appear in impurity-free vortices and are absent in defect-pinned vortices.

Second, the topological band structure of $FeTe_{0.55}Se_{0.45}$ originates from the k_z dispersion of the p_z orbital with odd parity, which anticrosses with the d_{xz} orbital with even parity along Γ–Z. A single topological band inversion occurs at Z, leading to a strong topological insulating phase in this compound[13–17]. However, under a larger amount of tellurium substitution, the p_z orbital may shift completely below the d_{xz} orbital along Γ–Z (refs. [14,48]), inducing a second topological band inversion around Γ. Consequently, Dirac surface states

disappear on the top surfaces of such a weak topological insulator, as previously proposed for the Fe(Te,Se) monolayer[14]. Indeed, two recent ARPES experiments observed the signature of topological band inversion around Γ on Fe(Te,Se) monolayers[49,50]. In our case, the intrinsic inhomogeneity[25–28] of $FeTe_{0.55}Se_{0.45}$ might cause the second topological band inversion around Γ to occur in some regions[48]. A more comprehensive discussion about the additional mechanisms of the presence or absence of MZMs in a vortex core is provided in Supplementary Section VI and Supplementary Fig. 10.

Online content

Any methods, additional references, Nature Research reporting summaries, source data, statements of code and data availability and associated accession codes are available at https://doi.org/10.1038/s41567-019-0630-5.

Data availability

The data that support the findings of this study are available from the corresponding authors on reasonable request.

Received: 20 November 2018; Accepted: 5 July 2019;
Published online: 19 August 2019

References

1. Nayak, C. et al. Non-Abelian anyons and topological quantum computation. *Rev. Mod. Phys.* **80**, 1083–1159 (2008).
2. Read, N. et al. Paired states of fermions in two dimensions with breaking of parity and time-reversal symmetries and the fractional quantum Hall effect. *Phys. Rev. B* **61**, 10267–10297 (2000).
3. Kitaev, A. Y. Unpaired Majorana fermions in quantum wires. *Phys. Uspekhi* **44**, 131–136 (2001).
4. Fu, L. & Kane, C. L. Superconducting proximity effect and Majorana fermions at the surface of a topological insulator. *Phys. Rev. Lett.* **100**, 096407 (2008).
5. Lutchyn, R. M., Sau, J. D. & Sarma, S. D. Majorana fermions and a topological phase transition in semiconductor–superconductor heterostructures. *Phys. Rev. Lett.* **105**, 077001 (2010).
6. Oreg, Y., Refael, G. & von Oppen, F. Helical liquids and Majorana bound states in quantum wires. *Phys. Rev. Lett.* **105**, 177002 (2010).
7. Mourik, V. et al. Signatures of Majorana fermions in hybrid superconductor–semiconductor nanowire devices. *Science* **336**, 1003–1007 (2012).
8. Nadj-Perge, S. et al. Observation of Majorana fermions in ferromagnetic atomic chains on a superconductor. *Science* **346**, 602–607 (2014).
9. Sun, H. H. et al. Majorana zero mode detected with spin selective Andreev reflection in the vortex of a topological superconductor. *Phys. Rev. Lett.* **116**, 257003 (2016).
10. Deng, M. T. et al. Majorana bound state in a coupled quantum-dot hybrid-nanowire system. *Science* **354**, 1557–1562 (2016).
11. Jeon, S. et al. Distinguishing a Majorana zero mode using spin-resolved measurements. *Science* **358**, 772–776 (2017).
12. Zhang, H. et al. Quantized Majorana conductance. *Nature* **556**, 74–79 (2018).
13. Wang, Z.-J. et al. Topological nature of the $FeSe_{0.5}Te_{0.5}$ superconductor. *Phys. Rev. B* **92**, 115119 (2015).
14. Wu, X.-X. et al. Topological characters in $Fe(Te_{1-x}Se_x)$ thin films. *Phys. Rev. B* **93**, 115129 (2016).
15. Xu, G. et al. Topological superconductivity on the surface of Fe-based superconductors. *Phys. Rev. Lett.* **117**, 047001 (2016).
16. Zhang, P. et al. Observation of topological superconductivity on the surface of iron-based superconductor. *Science* **360**, 182–186 (2018).
17. Wang, D. et al. Evidence for Majorana bound states in an iron-based superconductor. *Science* **362**, 333–335 (2018).
18. Liu, Q. et al. Robust and clean Majorana zero mode in the vortex core of high-temperature superconductor $(Li_{0.84}Fe_{0.16})$OHFeSe. *Phys. Rev. X* **8**, 041056 (2018).
19. Xu, J.-P. et al. Experimental detection of a Majorana mode in the core of a magnetic vortex inside a topological insulator–superconductor $Bi_2Te_3/NbSe_2$ heterostructure. *Phys. Rev. Lett.* **114**, 017001 (2015).
20. Rinott, S. et al. Tuning across the BCS–BEC crossover in the multiband superconductor $Fe_{1+y}Se_xTe_{1-x}$: an angle-resolved photoemission study. *Sci. Adv.* **3**, e1602372 (2017).
21. Hayashi, N. et al. Low-lying quasiparticle excitations around a vortex core in quantum limit. *Phys. Rev. Lett.* **80**, 2921–2924 (1998).
22. Caroli, C., de Gennes, P. G. & Matricon, J. Bound Fermion states on a vortex line in a type II superconductor. *Phys. Lett.* **9**, 307–309 (1964).
23. Gygi, F. & Schluter, M. Self-consistent electronic structure of a vortex line in a type-II superconductor. *Phys. Rev. B* **43**, 7609–7621 (1990).
24. Alicea, J. New directions in the pursuit of Majorana fermions in solid state systems. *Rep. Prog. Phys.* **75**, 076501 (2012).
25. He, X.-B. et al. Nanoscale chemical phase separation in $FeTe_{0.55}Se_{0.45}$ as seen via scanning tunneling spectroscopy. *Phys. Rev. B* **83**, 220502 (2011).
26. Lin, W.-Z. et al. Direct probe of interplay between local structure and superconductivity in $FeTe_{0.55}Se_{0.45}$. *ACS Nano* **7**, 2634–2641 (2013).
27. Singh, U. R. et al. Spatial inhomogeneity of the superconducting gap and order parameter in $FeSe_{0.4}Te_{0.6}$. *Phys. Rev. B* **88**, 155124 (2013).
28. Massee, F. et al. Imaging atomic-scale effects of high-energy ion irradiation on superconductivity and vortex pinning in Fe(Se,Te). *Sci. Adv.* **1**, e1500033 (2015).
29. Suderow, H. et al. Imaging superconducting vortex cores and lattices with a scanning tunneling microscope. *Supercond. Sci. Technol.* **27**, 063001 (2014).
30. Chen, M. et al. Discrete energy levels of Caroli–de Gennes–Martricon states in quantum limit in $FeTe_{0.55}Se_{0.45}$. *Nat. Commun.* **9**, 970 (2018).
31. Yin, Z. P., Haule, K. & Kotliar, G. Spin dynamics and orbital–antiphase pairing symmetry in iron-based superconductors. *Nat. Phys.* **10**, 845–850 (2014).
32. Khaymovich, I. M. et al. Vortex core states in superconducting graphene. *Phys. Rev. B* **79**, 224506 (2009).
33. Jackiw, R. & Rossi, P. Zero modes of the vortex–fermion system. *Nucl. Phys. B* **190**, 681–691 (1981).
34. Ghaemi, P. & Wilczek, F. Near-zero modes in superconducting graphene. *Phys. Scr.* **146**, 014019 (2012).
35. Colbert, J. & Lee, P. A. Proposal to measure the quasiparticle poisoning time of Majorana bound states. *Phys. Rev. B* **89**, 140505 (2014).
36. Liu, C.-X., Liu, D. E., Zhang, F.-C. & Chiu, C.-K. Protocol for reading out Majorana qubit and testing non-Abelian statistics. Preprint at https://arxiv.org/abs/1901.06083 (2019).
37. Shan, L. et al. Observation of ordered vortices with Andreev bound states in $Ba_{0.6}K_{0.4}Fe_2As_2$. *Nat. Phys.* **7**, 325–331 (2011).
38. Hanaguri, T. et al. Scanning tunneling microscopy/spectroscopy of vortices in LiFeAs. *Phys. Rev. B* **85**, 214505 (2012).
39. Hess, H. F., Robinson, R. B. & Waszczak, J. V. Vortex-core structure observed with a scanning tunneling microscopy. *Phys. Rev. Lett.* **64**, 2711–2714 (1990).
40. Kaneko, S.-I. et al. Quantum limiting behaviors of a vortex core in an anisotropic gap superconductor. *J. Phys. Soc. Jpn* **81**, 063701 (2012).
41. Coldea, A. I. & Watson, M. D. The key ingredients of the electronic structure of FeSe. *Annu. Rev. Condens. Matter Phys.* **9**, 125–146 (2018).
42. Hu, L.-H. et al. Theory of spin-selective Andreev reflection in the vortex core of a topological superconductor. *Phys. Rev. B* **94**, 224501 (2016).
43. Hasan, M. Z. & Kane, C. L. Colloquium: topological insulators. *Rev. Mod. Phys.* **82**, 3045–3067 (2010).
44. Schubert, G. et al. Fate of topological-insulator surface states under strong disorder. *Phys. Rev. B* **85**, 201105 (2012).
45. Sacksteder, V., Ohtsuki, T. & Kobayashi, K. Modification and control of topological insulator surface states using surface disorder. *Phys. Rev. Appl.* **3**, 064006 (2015).
46. Fu, L., Kane, C. L. & Mele, E. J. Topological insulators in three dimensions. *Phys. Rev. Lett.* **98**, 106803 (2007).
47. Noguchi, R. et al. A weak topological insulator state in quasi-one-dimensional bismuth iodide. *Nature* **566**, 518–522 (2019).
48. Qin, S.-S. et al. Topological vortex phase transitions in iron-based superconductors. Preprint at https://arxiv.org/abs/1901.03120 (2019).
49. Shi, X. et al. $FeTe_{1-x}Se_x$ monolayer films: towards the realization of high-temperature connate topological superconductivity. *Sci. Bull.* **62**, 503–507 (2017).
50. Peng, X.-L. et al. Observation of topological transition in high-T_c superconductor $FeTe_{1-x}Se_x/SrTiO_3(001)$ monolayers. Preprint at https://arxiv.org/abs/1903.05968 (2019).

Acknowledgements

We thank N.F. Yuan, C.-K. Chiu, C. Schrade, S.-S. Qin and R.-X. Zhang for helpful discussions and F.-Z. Yang, G.-J. Qian for technical assistance. The work at IOP is supported by grants from the Ministry of Science and Technology of China (2015CB921000, 2015CB921300 and 2016YFA0202300), the National Natural Science Foundation of China (11234014, 11574371 and 61390501), and the Chinese Academy of Sciences (XDB28000000 and XDB07000000). L.F. and G.D.G are supported by US DOE (DE-SC0010526 and DE-SC0012704, respectively). J.S. and R.D.Z. are supported by the Center for Emergent Superconductivity, an EFRC funded by the US DOE.

Author contributions

H.D. and H.-J.G. designed the experiments. S.Z., L.C., H.C. and Y.X. performed the STM experiments with assistance from L.K., W.L., D.W., P.F. and S.D. M.P., H.I. and L.F. provided theoretical models and simulations. J.S., R.Z. and G.D.G. provided samples. L.K., S.Z. and H.D. analysed experiment data with input from all other authors. L.K.,

M.P. and S.Z. plotted figures with input from all other authors. All authors participated in writing the manuscript. H.D., H.-J.G. and L.F. supervised the project.

Competing interests

The authors declare no competing interests.

Additional information

Supplementary information is available for this paper at https://doi.org/10.1038/s41567-019-0630-5.

Reprints and permissions information is available at www.nature.com/reprints.

Correspondence and requests for materials should be addressed to L.F., H.-J.G. or H.D.

Peer review information: *Nature Physics* thanks Peter Wahl and the other, anonymous, reviewer(s) for their contribution to the peer review of this work.